Enhanced visible-light photoreduction of CO_2 to methanol over Mo_2C/TiO_2 surfaces in an optofluidic microreactor

Jonathan Albo[1,*], Gonzalo García[2]

[1] Department of Chemical & Biomolecular Engineering, University of Cantabria (UC), Avda. Los Castros s/n, 39005. Santander, Spain

[2] Instituto de Materiales y Nanotecnología, Departamento de Química, Universidad de La Laguna, PO Box 456, 38200, La Laguna, Santa Cruz de Tenerife, Spain

*Corresponding author; e-mail: jonathan.albo@unican.es

Abstract

Inspired by the photosynthesis process used by plants, the photocatalytic conversion of CO_2 with water to obtain chemical energy can tackle increasing CO_2 emissions and energy demand together. In this work, the performance of Mo_2C/TiO_2 blends in the continuous photocatalytic reduction of CO_2 to methanol is evaluated in a micro-optofluidic reactor illuminated with UV and visible LED lights (5 $mW \cdot cm^{-2}$). The photo-responsive Mo_2C/TiO_2 surfaces applied are manufactured by airbrushing a photocatalytic ink containing different weight percent (2-10%) of Mo_2C nanoparticles (synthesized by a carbothermal method) and TiO_2 (P25) onto porous carbon papers. Doping TiO_2 with Mo_2C makes the composite material to present activity in the visible region compared with bare TiO_2, while it does not bring performance enhancements when the photoactive surfaces are illuminated with UV light. A 4% Mo_2C weight percent led to an enhanced stable production of methanol under visible light (r= 11.8 $\mu mol \cdot g^{-1} \cdot h^{-1}$, AQY= 0.21%, $S_{CH3OH/HCOOH}$= 12.1), which is ascribed to the presence of Mo_2C, able to extend the spectral response, as well as reduce the recombination rate of photogenerated electrons and holes occurring in TiO_2. Higher Mo_2C contents, however, seem to shield the photoexciting capacity of TiO_2.

Keywords: CO_2 reduction, photocatalysis, Mo_2C/TiO_2, optofluidic microreactor, methanol.

1. Introduction

With the inexorable rise of CO_2 concentration in the atmosphere, which has already exceeded 411 ppm in September 2020,[1] CO_2 chemistry has become a very attractive area of research, not

only for environmental reasons, but also due to the potential use of CO_2 as an alternative and non-toxic economical feedstock for the generation of value-added products, such as alcohols.[2-4] In particular, the reduction of CO_2 towards methanol (CH_3OH), a satisfying initial product from CO_2 due to its suitability for near-term implementation,[5] is being concerned increasingly as a high-efficiency chemical storage carrier for H_2 derived from renewable sources (e.g., H_2O), as well as a key platform chemical for various useable products such as gasoline, olefins, biodiesel and fuel additive.[6] The activation of CO_2 is, however, quite challenging due to the stability of CO_2 that requires of suitable catalysts with active sites for CO_2 adsorption and ample amount of energy. Some of the reported CO_2 activation processes for CH_3OH production are energy intensive (high temperatures and pressures), and so the research community is putting the efforts on developing more sustainable processes that can proceed at mild conditions, such as the electrochemical or photochemical CO_2 conversion pathways.[7-10] The latter, the photocatalytic conversion of CO_2 with water to obtain chemical energy (also known as artificial photosynthesis) permits the conversion of CO_2 under mild conditions without additional energy input (except for the solar irradiation) and has received increasing attention due to its potential environmental and economic benefits (tackling increasing CO_2 emissions and energy demand together).

Because of its high photo-stability, non-toxicity and low-cost, TiO_2 has been widely applied as semiconductor for solar-fuel production, and particularly for the formation of CH_3OH.[11,12] Unfortunately, TiO_2 possesses a large band gap (~ 3 eV), which makes it active under UV light whereas the UV light constitutes only ~4% of solar spectrum. Thus, the poor ability of TiO_2 in absorbing visible light, which is the main part of the sunlight (~ 44%), is one of the origins for the low photocatalytic efficiency. The effectiveness of TiO_2 for CO_2 photoreduction is also limited by its high electron-hole recombination rate. Several strategies have been developed to overcome these above-mentioned problems, so TiO_2 can be effective in the visible region and separate the photogenerated charges. Among them, doping TiO_2 with metals and coupling it with other semiconductors can be an effective and direct way to promote charge separation, CO_2 activation and selective formation of reaction products, inhibiting the back-recombination reaction.[13] Particularly, molybdenum carbide (Mo_2C) has demonstrated to be quite useful for the catalytic conversion of CO_2 to CH_3OH because of its dual functionality for H_2 dissociation and C=O bond scission, usually showing superior catalytic properties than noble metals in terms of selectivity, stability and resistance to poisoning.[14-23] Besides, Mo_2C is able to enhance photocatalytic activity in different systems under visible light, boosting photo-generated charge

carriers transportation.[24-29] Thus, the use of Mo_2C/TiO_2 composites may be a good approach to enhance the activity of TiO_2 in the photocatalytic conversion of CO_2 to CH_3OH. In addition, the carbides are conductive, benefiting for the charge separation in photocatalysis and increasing also the lifetime of the photogenerated electron-hole pairs.[22,30] The photocatalytic activity of Mo_2C/TiO_2 has been, however, rarely reported in the literature.[25,31-33]

Furthermore, an efficient system for the photocatalytic transformation of CO_2 to CH_3OH may not only take into account the photoactive material but the photoreactor design, trying always to effectively harness light irradiation, optimising exposure of active sites and minimizing mass transfer constraints. In this regard, the use of optofluidic microreactors may bring several advantages in the photocatalytic reduction of CO_2, including large surface-area-to-volume ratio, uniform light distribution, enhanced mass transfer and fine flow control,[34] in contrast to common slurry batch-type reactors that have been demonstrated to be inefficient to induce the challenging reaction to form CH_3OH,[35] due to a low surface-area-to-volume ratio because of particle agglomeration, and the required separation of the photocatalyst material from obtained products. In fact, planar microreactor configurations have already exhibited superior performance in various photocatalytic processes,[36,37] including CO_2 photoreduction.[38-43]

The aim of this work is to evaluate the performance of Mo_2C/TiO_2 blends in the continuous photocatalytic reduction of CO_2. Mo_2C is synthesized by a carbothermal method. This synthetic route allows the large-scale production of nanoparticles with a considerable small size, high crystallinity and purity.[44,45] The work includes the effect of applying Mo_2C/TiO_2 blends with different weight percent of Mo_2C in the CO_2-to-CH_3OH reaction using a micro-optofluidic reactor illuminated with UV and visible LED lights. The results may help in developing more efficient materials and devices for the photocatalytic reduction of CO_2.

2. Experimental

2.1. Synthesis and physicochemical characterization of the materials

The nanometric Mo_2C particles are synthesized by a slight modification of a standard carbothermal method.[46] Briefly, an appropriate amount (e.g. 1.8 g) of molybdenum oxide precursor (MoO_3, 99.5% Sigma-Aldrich) is dissolved in the correct volume of ammonium hydroxide solution (e.g. 30 mL of 15% of NH_4OH solution, 99.99% Sigma-Aldrich) under stirring at room temperature ("Sample A"). "Sample B" consists of a suspension of the appropriate amount (e.g. 0.15 g) of carbon black (Vulcan® XC 72R) in a correct volume (e.g.

30 mL) of ethanol (CH_3CH_2OH, Merck p.a.) prepared by sonication. “Sample A” is added drop by drop into “Sample B” under stirring at room temperature and then the temperature is raised up to 60 °C until a dry powder is achieved. Finally, the sample is grounded in a mortar and subsequently introduced in a tubular furnace under a H_2/N_2 (5 vol.%) flow (140 $mL \cdot min^{-1}$), in which a ramp of 5 $°C \cdot min^{-1}$ from room temperature to 800 °C is applied. The highest temperature (800 °C) is maintained during a period of 10 h and, after that, the temperature is cooled down to room temperature under the same temperature ramp and flow conditions.

Subsequently, different amounts of the synthesized Mo_2C nanoparticles (2-10 wt.%) were mixed with TiO_2 (P25 ≥ 99.5% Sigma-Aldrich) to obtain Mo_2C/TiO_2 blends. Table 1 shows the nomenclature, together with the corresponding mass composition of the Mo_2C, TiO_2 and Mo_2C/TiO_2 blends applied as determined by Microwave Plasma Atomic Emission Spectroscopy (MP-AES 4200 Agilent Technologies). Commercial Mo_2C particles were also acquired (99.5% Sigma-Aldrich) and applied for comparison.

Table 1. Composition of the photocatalysts applied

Material	**Nomenclature**	**Mass ratio (%)**	
		Mo_2C	**TiO_2**
Mo_2C (commercial)	Mo_2C (commercial)	100	-
Mo_2C (carbothermal)	Mo_2C	100	-
Mo_2C/TiO_2	Mo_2C2	2.2	97.8
	Mo_2C4	4.3	95.7
	Mo_2C6	5.7	94.3
	Mo_2C10	9.6	90.4
TiO_2	TiO_2	-	100

XRD powder spectra were acquired from X’Pert PRO X-ray diffractometer (PANalytical) to determine the crystal structure. Measurements were obtained using the CuKα radiation (λ = 1.5405 Å) and the X’pert high score plus diffraction software, and 2θ data were collected from 20° to 100° with a scanning rate of 0.04° s^{-1}. Crystalline phases were identified by comparing the experimental diffraction patterns with the Joint Committee on Powder Diffraction Standards (JCPDS). Raman spectra were collected using a SPELEC RAMAN (Metrohm DropSens) instrument with a green laser (λ = 532 nm) in the 100 to 3200 cm^{-1} range. Besides, the diffuse

reflectance in UV-VIS-NIR region was measured with a spectrophotometer (Agilent Technologies Cary 5000).

2.2. Preparation and characterization of the light-responsive surfaces

The photo-responsive surfaces applied are manufactured by airbrushing a photocatalytic ink (containing Mo_2C, TiO_2 or Mo_2C/TiO_2 mixtures) onto porous carbon paper (TGP-H60, Toray Inc.) covered by a paper mask with a hole of 1 cm^2. This chemically stable substrate is able to minimize transport resistance, contributing to an efficient transfer of CO_2 and diffusion of products.[47,48] The ink includes a Nafion® dispersion of 5wt.% (Alfa Aesar) as binder and isopropanol (IPA) (Sigma Aldrich) as a vehicle, with a 70/30 catalyst/Nafion mass ratio and a 3% of solids (catalyst + Nafion) percentage. The surfaces present a photocatalytic loading of L = 2 $mg \cdot cm^{-2}$ prepared by simple accumulation of layers and complete IPA evaporation at 100 ºC on a heating plate. The materials were dried at ambient conditions for 24 hours and rinsed with deionised water before their employment in a planar optofluidic microreactor (APRIA Systems S.L.). The photoactive materials are placed in the centre of the reaction chamber and are irradiated with 1200 mW UV (365 nm) or visible (450 nm) LED lights with a light intensity of E= 5 $mW \cdot cm^{-2}$ measured by a radiometer (Photoradiometer Delta OHM). The experimental setup has been described in detail elsewhere.[38]

A CO_2 saturated 0.5 M $KHCO_3$ (Panreac >97%) aqueous solutions was prepared with ultra-pure water (18.2 MΩ cm at 273 K, MilliQ Millipore system) and supplied to the liquid microchamber with a peristaltic pump (Miniplus 3 Gilson) at a flow rate of Q_L= 50 $\mu L \cdot min^{-1}$. The experiments were carried out in continuous mode under ambient temperature and pressure conditions. The microcell was placed in a ventilated dark box and temperature was controlled with an infrared thermometer to ensure an ambient temperature (~25ºC) during the experimental time. Liquid samples were taken every 30 min and for 120 min from the collection vessel placed at the outlet of the microreactor. The concentration of alcohols in each sample was analysed by duplicate in a headspace gas chromatograph (GCMS-QP2010 Ultra Shimadzu) equipped with a flame ionization detector (FID). Additionally, formate ($HCOO^-$) concentration was analysed in duplicate by Ion Chromatography (Dionex ICS 1100). An average concentration was obtained for each point from the performance of three replicates with an experimental error less than 16.1 %. The photocatalytic performance is analysed in terms of r (i.e., yield per gram of material and time), apparent quantum yield, AQY, defined as the rate of electrons transferred towards CH_3OH per rate of incident photons, and selectivity, S, as the ratio

between reaction rate for CH_3OH and the reaction rate for the other detected liquid product, HCOOH.

3. Results and discussion

3.1. Characterization of the Mo_2C/TiO_2-based surfaces

The bare synthesized and commercial Mo_2C materials have been fully characterized in previous reports.[45,46] The characterization results for the Mo_2C/TiO_2 mixtures applied are presented hereafter.

Figure 1 shows XRD patterns of Mo_2C/TiO_2 mixtures. All samples showed the presence of both anatase and rutile TiO_2 crystalline phases, which is desired for optimal photocatalytic activity.[49] It can be also observed small, but visible, diffraction patterns of Mo_2C. The most intense signals are related to anatase (JCPDS no. 21-1272), which has diffraction peaks at 2θ = 25.20º, 36.88º, 37.74º, 38.48º, 47.97º, 53.87º, 54.99º, 62.40º, 68.68º, 70.39º and 75.00º, corresponding to the reflection from (103), (004), (112), (200), (105), (211), (204), (116), (220) and (215) crystal planes. Rutile (JCPDS no. 21-1276) reveals diffraction peaks at 2θ = 27.34º, 36.00º, 41.18º, 54.21º, 56.56º, 62.67º, 68.91º and 70.20º associated with the reflection from (110), (101), (111), (211), (220), (002), (301) and (002) crystal planes. Mo_2C (JCPDS no. 01-1188) depicts diffraction peaks at 2θ = 34.30º, 37.81º, 39.35º, 52.07º, 61.56º, 69.58º, 74.71º and 76.00º related to the reflection from (100), (002), (101), (102), (110), (103), (112) and (201) crystal planes. The Debye-Scherrer equation was used to estimate the crystallite size of Mo_2C and TiO_2. Average metal crystallite sizes of 20.35 nm and 30.79 nm were calculated from the largest peaks at 25.20º (anatase phase) and at 34.30º (Mo_2C), respectively. Additionally, the position of all diffraction peaks is similar for all the samples. Therefore, crystalline structure of TiO_2 and Mo_2C remains similar for all Mo_2C/TiO_2 mixtures.

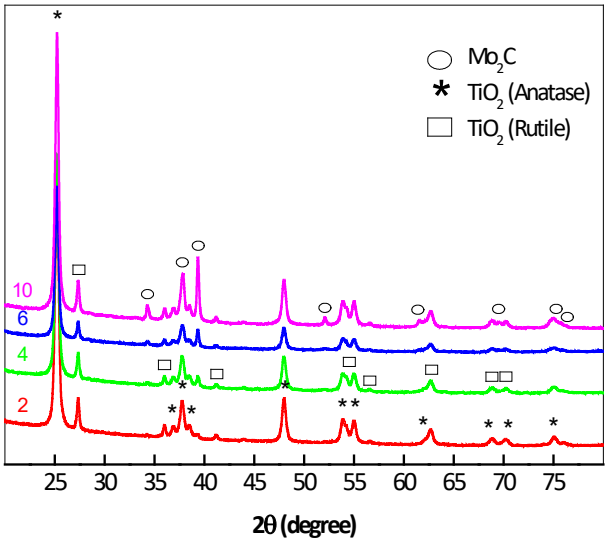

Figure 1. XRD patterns of Mo_2C2 (in black), Mo_2C4 (in red), Mo_2C6 (in green) and Mo_2C10 (in blue) materials.

Moreover, Figure 2 shows Raman spectra of the Mo_2C/TiO_2 mixtures in comparison to commercial TiO_2.

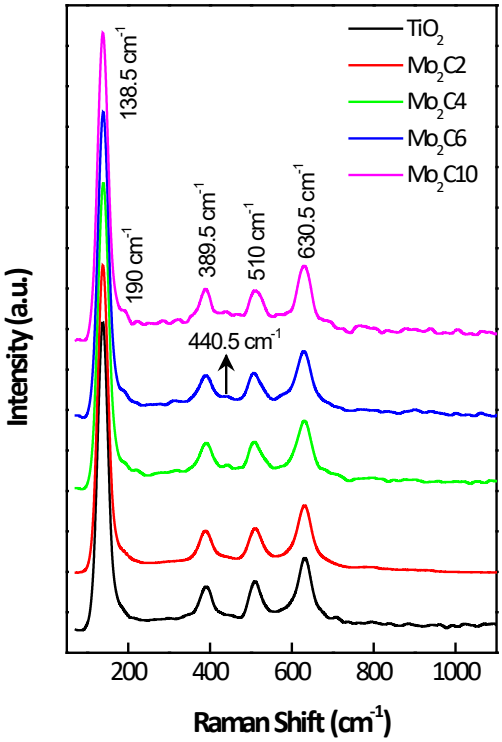

Figure 2. Raman spectra of Mo_2C/TiO_2 composites and TiO_2.

Raman spectra reveal typical peaks of anatase phase, i.e. 138.5 cm^{-1}: E_g; 190 cm^{-1}: E_g; 389.5 cm^{-1}: B_{1g}; 510 cm^{-1}: (B_{1g} + A_{1g}); and 630.5 cm^{-1}: E_g.[50] The peak at 440.5 cm^{-1} is the weakest and it is associated to the E_g mode of the rutile phase.[51] This is consistent with XRD analyses (Figure 1). Interestingly, Raman spectra of Mo_2C is not visible at Mo_2C/TiO_2 mixtures; however, the whole Raman intensity decreases with the Mo_2C content in the sample. It is important to note that the as-synthesized Mo_2C materials develop a metal crystallite size of ca. 30 nm and consist of core-shell particles with a pure Mo_2C core and a small shell (2–3 nm) containing molybdenum oxide species.[44] The small quantity of these oxide species appears to be below the detection limit of the Raman equipment. On the other hand, the strongest, well resolved Raman active mode (138.5 cm^{-1}) is due to the external vibrations of the anatase structure, which is typically employed as a sign of long-range order.[52] The rest of the Raman peaks are weakly broadened and insignificant variations in their relative intensities can be observed. Specifically, the band at 138.5 cm^{-1} is associated with O–Ti–O symmetric stretching vibrations, which can be used to estimate the interaction with the surrounding medium. Indeed, E_g modes are more sensitive to the concentration of oxygen vacancies in TiO_2, as they are related to planar O–O interactions.[51] The position and the full width at half maximum (FWHM) of the Raman bands can be analyzed on the basis of the changes in the stoichiometry and defects caused by Mo_2C content.[50-52] In this regard, the position and the FWHM of the E_g-band (138.5 cm^{-1}) with the Mo_2C loading is given in Figure 3.

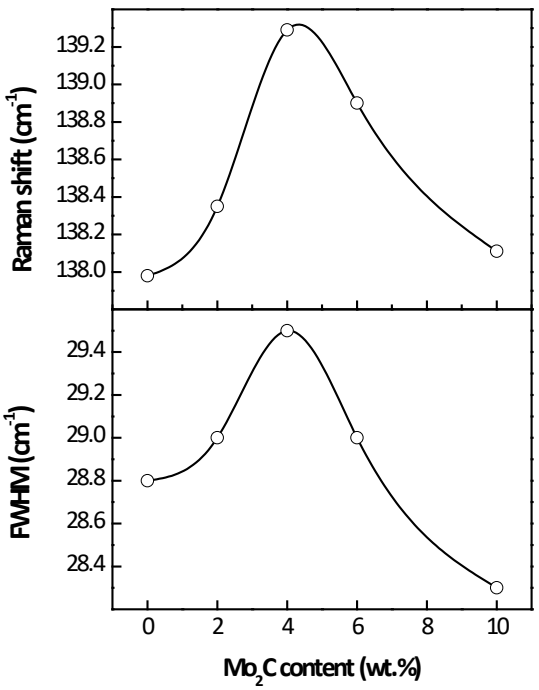

Figure 3. Shift in E_g-band position (top panel) and broadening of the E_g-band with the Mo_2C content.

It can be discerned that both parameters depict a bell-shaped curve with a maximum when the sample contains 4% Mo_2C (Mo_2C4). The last suggests a contraction of O–Ti–O bonds with the amount of Mo_2C into the Mo_2C/TiO_2 mixtures up to 4% of Mo_2C loading. Besides, UV–Vis diffuse reflectance spectroscopy (Figure 4) showed that the absorption band edge for TiO_2 is around 400 nm and the addition of Mo_2C makes the absorption increasing at longer wavelengths (visible range), as observed from the absorption edge of 480 nm with Mo_2C10. It can be also seen that increases in Mo_2C content led to an enhanced absorbance, which agrees well with previous reports.[24-29] Figure 4b shows the estimated optical bandgap energies of the samples as calculated by Kubelka- Munk method ($[F(\text{reflectance, R})h\nu]^2$ vs. photon energy ($h\nu$)). Low bandgap energy values ranging from 3.22 and 3.36 eV can be obtained for Mo_2C/TiO_2 composites compared to 3.48 eV for TiO_2. The narrowing in bandgap energy with Mo_2C content can be linked to an improved electronic properties of the composites as a result of the Mo_2C-TiO_2 interaction.

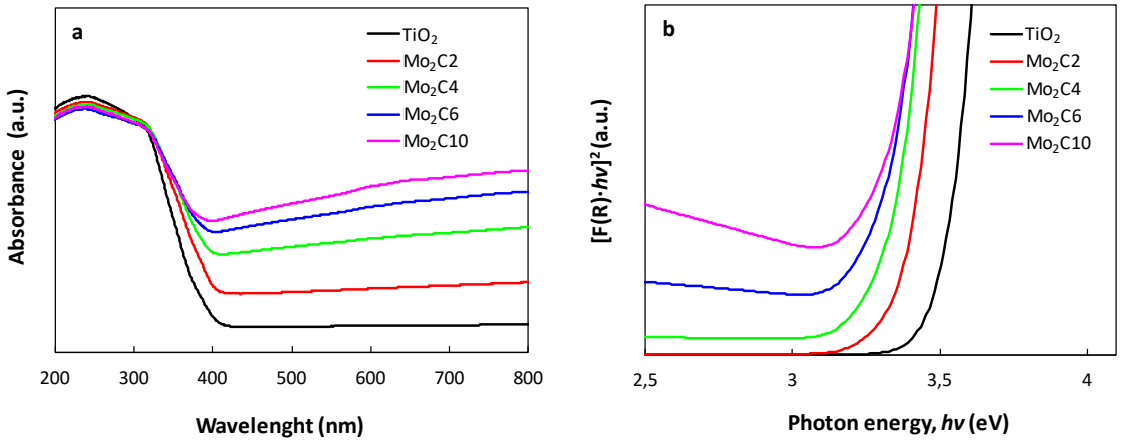

Figure 4. (a) UV-Vis absorption spectra and, (b) bandgap energies plot (Kubelka-Munk function) of Mo_2C/TiO_2 mixtures in comparison to TiO_2.

3.2. Continuous transformation of CO_2 in the planar optofludic microreactor

The continuous photocatalytic reduction of CO_2 in the micro-optofluidic reactor was firstly evaluated at the synthesized and commercial Mo_2C-based surfaces and the results are presented in Table 2. Blank tests were also conducted in the dark and the absence of CO_2 and no measurable liquid products were detected. Gas phase reduction productions were not analysed.

Table 2. CO_2 conversion to liquid products at Mo_2C-based photoactive surfaces

Material	Light	r (μmol·g^{-1}·h^{-1})		$S_{CH_3OH/HCOOH}$ (-)
		CH₃OH	*HCOOH*	
Mo_2C	UV	0.04	0.02	2
	Vis	0.11	0.03	3.7
Mo_2C (commercial)	UV	-	-	-
	Vis	-	-	-

The synthesized Mo_2C nanoparticles led to the formation of CH_3OH, with also small quantities of HCOOH, as a potential intermediate in the CO_2-to-CH_3OH conversion pathway.[10] The formation of CH_3OH is somehow expected if we consider the literature on the catalytic conversion of CO_2 at Mo_2C-based surfaces, which can be associated with the dual functionality for H_2 dissociation and C=O bond scission.[14-23] As observed, the rate for CH_3OH formation and reaction selectivity are higher when visible light illuminated the photoactive surfaces (r= 0.11 μmol·g^{-1}·h^{-1} and $S_{CH_3OH/HCOOH}$= 3.7) in comparison to the performance under UV light irradiation (r= 0.04 μmol·g^{-1}·h^{-1} and $S_{CH_3OH/HCOOH}$= 2), which can be related to the ability of Mo_2C to enhance the photocatalytic activity with visible light.[24-29] Besides, the system is able to produce CH_3OH, in contrast to previous results at CdS/Mo_2C nanowires that tend to be very selective to the formation of hydrogen-deficient carbon products (98.3% for CO) from the photoreduction of CO_2,[53] which might be linked to the presence of CdS. Conversely, a previous report shows that CH_3OH can be produced at high concentrations (463.68 mg L^{-1}) when applying MoS_2 rods-TiO_2 nanotubes heterojunction electrodes in the photo-assisted electrocatalytic reduction of CO_2.[54] Anyhow, the CH_3OH concentrations obtained in this work are limited and the main reduction products are probably CO and CH_4, as commonly found in other Mo-based systems applied in the photocatalytic reduction of CO_2.[55-60]

All in all, the results reveal the potential of the Mo_2C nanoparticles synthesized by a carborthermal method for CH_3OH formation, as well as the positive effect of applying a planar optofluidic microreactor configuration with enhanced mass transport, larger volume/active area ratio and uniform light distribution. Furthermore, no liquids products can be detected when using the commercial Mo_2C particles supported in the porous carbon papers, and so the synthesized Mo_2C nanoparticles are used hereafter for testing the performance of the Mo_2C/TiO_2 blends.

Figure 5a and 5b show the effect of Mo_2C weight percent in the Mo_2C/TiO_2 blends on CH_3OH and HCOOH production rates after 2 hour of UV or visible light illumination (E= 5 mW·cm^{-2}), respectively.

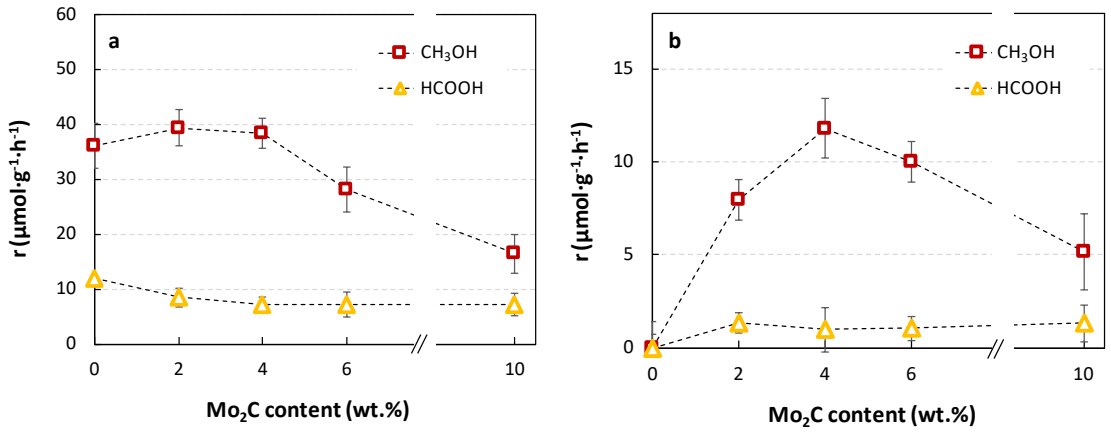

Figure 5. Yields for CH_3OH and HCOOH under (a) UV and (b) visible light illumination

The results firstly show that mixing Mo_2C with TiO_2 does not bring performance enhancements when the photoactive surfaces are illuminated with UV light, in comparison with the yields observed at bare TiO_2. In fact, a Mo_2C weight percent higher than 4% seem to shield the photoexciting capacity of TiO_2, weakening photocatalytic activity for CH_3OH formation. Nevertheless, mixing TiO_2 with Mo_2C makes the material to present activity in the visible region (no CH_3OH was detected with TiO_2). Thus, doping Mo_2C onto TiO_2 may be responsible for the visible light activity, which can be related to the ability of Mo_2C to enhance the photocatalytic activity under visible light. The yields for CH_3OH find a maximum when the Mo_2C/TiO_2 photoactive surfaces contain 4% Mo_2C (Mo_2C4) and are irradiated with visible light. At this optimal point, CH_3OH yield can be as high as r= 11.8 µmol·g^{-1}·h^{-1} (AQY= 0.21 %) after 2 hours of illumination (Figure 5b). This optimal performance with Mo_2C4 is in agreement with Figure 2 and Figure 3 where the shift and the broadening of the Raman band with Mo_2C loading appear as the main reasons for visible light activity, which is maximum at the maximum contraction of O–Ti–O bonds. The increase of photocatalytic activity with Mo_2C content can be ascribed with a reduction in the band-gap energy, which enhanced the excitation of electrons from the valence band to the conduction band (Figure 4). That is to say, the photoelectrons are generated from TiO_2 and transferred across the interface between TiO_2 and Mo_2C to the surface of Mo_2C, leaving the photogenerated holes in the valence band of TiO_2. When the photogenerated electrons are trapped by Mo_2C particles, electron–hole pairs are efficiently

separated, and CO_2 reduction can be enhanced.[33] Thus, by combining Mo_2C with TiO_2 is possible to effectively extend the spectral response properties of TiO_2, improving the interfacial conductivity (because of the high electrical conductivity of Mo_2C), facilitating the transport of photogenerated charge carriers to the active sites and reducing the recombination rate of photogenerated electrons-holes and thus increasing the photoefficiency.[25,32,33] Besides, the literature demonstrated that Mo_2C can provide active sites for CO_2 adsorption and activation. With more CO_2 adsorbed on the photocatalyst, more CO_2 (reactant) will participate in the forward reaction, which is beneficial for shifting the chemical equilibrium toward the reduction products.[53] It is also worth mentioning that the values obtained in this work with Mo_2C4 agree well with the optimum 3-4% Mo weight percent found in other Mo-based systems for the photocatalytic conversion of CO_2.[24-29]

Moreover, Figure 6 shows reaction selectivity to produce CH_3OH over HCOOH ($S_{CH_3OH/HCOOH}$) from the continuous photoreduction of CO_2 in the planar microreactor.

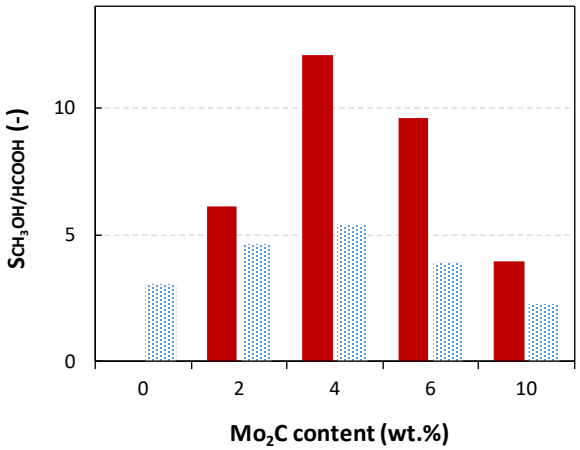

Figure 6. Selectivity to CH_3OH in the photocatalytic reduction of CO_2 at different Mo_2C contents under UV (in blue) and visible light (in red).

The results presented in Figure 6 evidence that Mo_2C content has also a marked effect on reaction selectivity at the Mo_2C/TiO_2-based photoactive surfaces developed. In particular, the data show again that the use of Mo_2C4 led to a more selective transformation of CO_2 to CH_3OH over HCOOH production under visible light, with a $S_{CH_3OH/HCOOH}$= 12.1. The same can be said when the surfaces are irradiated under UV light, although the effect is clearly less pronounced. Exceeding a 4 wt.% Mo_2C content, the photocatalyst tends to diminish CH_3OH production while it slightly enhances the production of HCOOH per gram of material. This indicates that the amount of Mo_2C active sites in the photoactive surface have a critical influence on reaction

selectivity (and so in reaction mechanisms). Certainly, an in-depth study on reaction mechanisms is required in order to elucidate and control reaction selectivity in the photoconversion of CO_2 to CH_3OH at Mo_2C/TiO_2-based surfaces.

Finally, Figure 7a shows the yields for CH_3OH at longer irradiation times, while Figure 7b shows the rates obtained with time and in three consecutive runs for Mo_2C4 photocatalyst. The reaction solution was changed after each run.

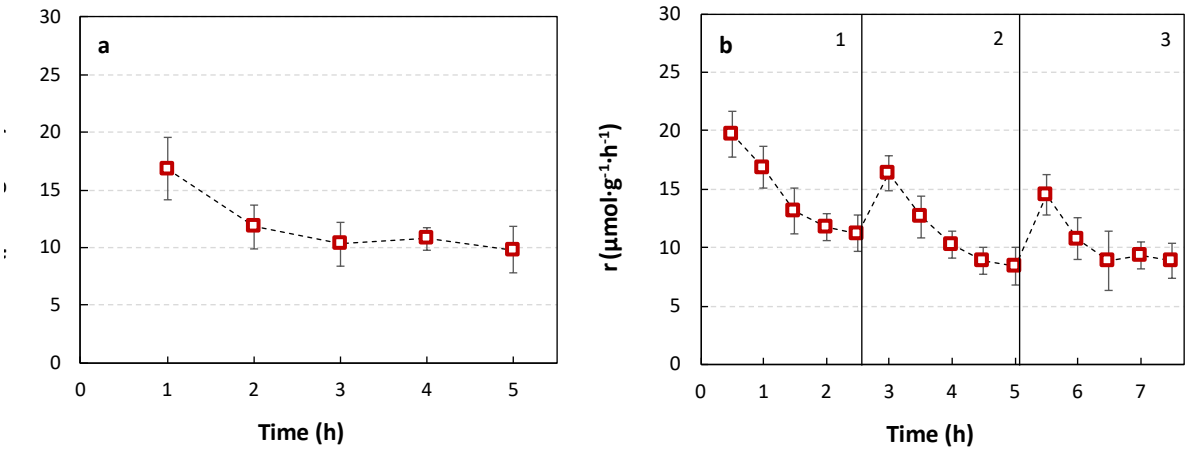

Figure 7. Time-dependence for the (a) photocatalytic production of CH_3OH using Mo_2C4 and (b) after three consecutive runs under visible light.

As observed, the activity of Mo_2C4 decays more abruptly during the first 2 hours of irradiation with visible light going from a r= 16.9 μmol·g^{-1}·h^{-1} to r=11.8 μmol·g^{-1}·h^{-1}. The phenomenon of reduction in the photocatalytic conversion of CO_2 at longer periods of time is usually ascribed to the reduction in photocatalyst ability to absorb light or the formation of un-desorbed products over the active sites.[61] In any case, the results show that after the first 2 hours of photoreduction of CO_2, the rate to produce CH_3OH remains relatively steady up to 5 hours of continuous operation.

Besides, Figure 7b shows how the yields decay slowly after three consecutive runs of 2.5 hours, which can be ascribed to the aforementioned effects, as well as material leaching as reported before with catalytic materials supported onto porous carbon supports by spray-coating.[47,48] Despite that, the increase at the initial stage of each cycle suggests that the activity loss is also determined by the blocking of the photocatalytic sites, which is mitigated from one cycle to the other upon washing of the material. Thus, CH_3OH yield at the initial stage of the second cycle is 83 % of the initial yield in the first one, and results in 74% in the third run. However, the

reaction rates hardly changed (r=~9 μmol·g^{-1}·h^{-1}) after 2.5 hours of visible light illumination in the second and third cycle, which denotes the recyclability and stability of the Mo_2C/TiO_2 material during irradiation.

Overall, the Mo_2C4-based photoactive surfaces could remain quite stable in the conversion of CO_2 to CH_3OH in the planar optofluidic microreactor applied under visible light illumination, with a maximum yield to CH_3OH of r= 11.8 μmol·g^{-1}·h^{-1} (AQY= 0.21 %) and selectivity over HCOOH of $S_{CH3OH/HCOOH}$= 12.1. These values are, of course, far from a real application, but the enhancement in CO_2 conversion under visible light looks promising and can be considered a step further in the field.

4. Conclusions

With this work, an extensive photocatalytic study on the reduction of CO_2 on Mo_2C/TiO_2 blends in a micro-optofluidic reactor illuminated with UV and visible LED lights has been performed. The main conclusions drawn from the study can be summarized as follows:

- The use of commercial Mo_2C nanoparticles do not lead to the formation of liquid products from CO_2 photoreduction, while synthesized Mo_2C nanoparticles by a carbothermal method can generate small amounts of methanol and formic acid under UV and visible irradiation.

- Mixing TiO_2 with the synthesized Mo_2C nanoparticles strongly enhances the photocatalytic production of methanol under visible light (TiO_2 is only photoactive under UV irradiation). Mo_2C/TiO_2 blends containing 4 wt. % of Mo_2C nanoparticles reveals the best performance for methanol production visible light irradiation (r= 11.8 μmol·g^{-1}·h^{-1}, AQY= 0.21%, $S_{CH3OH/HCOOH}$= 12.1).

- The Mo_2C/TiO_2 material presents elevated photocatalytic stability and recyclability under visible irradiation.

The main reasons for all these outcomes can be related to a reduction in the band-gap energy, efficient separation of electron-hole pairs, and improved interfacial conductivity. Besides, the amount of Mo_2C nanoparticles modulates the O-Ti-O bond strength, being the maximum photocatalytic activity at the maximum bond contraction (4 wt. % of Mo_2C).

All in all, mixing nanostructured transition metal carbides with TiO_2 under visible light appears as a promising strategy to develop novel photocatalysts for an enhanced CO_2 photoreduction to methanol.

Acknowledgments

The authors gratefully acknowledge the financial support from the Spanish Ministry of Science and Innovation (MICINN) under Ramón y Cajal programme (RYC-2015-17080), PID2019-104050RA-I00 and ENE2017-83976-C2-2-R. G.G. acknowledges the "Viera y Clavijo" program (ACIISI & ULL). Authors would also like to thank the use of SEGAI—ULL facilities and the Laser Spectroscopy and High Pressure Group (ULL) for diffuse reflectance measurements.

References

[1] Mauna Loa Observatory – National Oceanic and Atmospheric Administration (NOAA), https://www.esrl.noaa.gov/gmd/ccgg/trends/monthly.html (accessed 17 September 2020).

[2] J. Albo, M. Perfecto-Irigaray, G. Beobide, A. Irabien, *J. CO2 Util*., 2019, **33**, 157-165.

[3] J. Albo, D. Vallejo, G. Beobide, O. Castillo, P. Castaño, A. Irabien, *ChemSusChem*, 2017, **10**, 1100 –1109.

[4] J. Albo, G. Beobide, P. Castaño, A. Irabien, *J. CO2 Util*., 2017, **18**, 164-172.

[5] R. Chauvy, N. Meunier, D. Thomas, G. De Weireld, *Appl. Energ*., 2019, **236**, 662–680.

[6] G. A. Olah, A. Goeppert, G. K. S. Prakash, *J. Org. Chem.,* 2009, **74***:* **2**, 487-498.

[7] J. Albo, M. Alvarez-Guerra, A. Irabien, Electro-, Photo-, and Photo-electrochemical reduction of CO_2, in: W. Y. Teoh, A. Urakawa, Y. H. Ng and P. H. –L. Sit (Ed.), Heterogeneous Catalysts: Emerging Techniques for Design, Characterization and Applications. *Wiley-VCH GmbH*, Weinheim, 2021, ISBN: 13: 978-3527344154.

[8] G. Chen, G. I. N. Waterhouse, R. Shi, J. Zhao, Z. Li, L. Z. Wu, C. H. Tung, T. Zhang, *Angew. Chem. Int. Edit*., 2019, **58, 49**, 17528-17551.

[9] Albo, J. Photocatalytic synthesis of methanol from CO_2 and H_2O, in: J. Albo (Ed.), Carbon Dioxide Capture: Processes, Technology and Environmental Implications. *Nova Publishers*, New York, 2016, 277–300. ISBN: 978-163485321-7.

[10] J. Albo, M. Alvarez-Guerra, P. Castaño, A. Irabien, *Green Chem*., 2015, **17(4)**, 2304-2324.

[11] Y. Ma, X. Wang, Y. Jia,, X. Chen, H. Han, C. Li, *Chem. Rev*., 2014, **114**, 9987-10043.

[12] S. N. Habisreutinger, L. Schmidt-Mende, J. K. Stolarczyk, *Angew. Chem. Int. Ed*., 2013, **52**, 7372–7408.

[13] W. Tu, Y. Zhou, Z. Zou, *Adv. Mater.,* 2014, **26**, 4607−4626.

[14] A. A. Garcia Blanco, O. J. Furlong, D. J. Stacchiola, K. Sapag,, M. S. Nazzarro, *Top. Catal*., 2019, **62**, 1026-1034.

[15] H. Han, G. Wenhao, X. Linfei, W. Wei, *J. Taiwan Inst. Chem. E*., 2019, **95**, 112-118.

[16] K. S. Reddy, S. Dama, N. B. Mhamane, M. J. Ghosalya, T. Raja, C. V. Satyanarayana, C. S. Gopinath, *Dalton Trans*., 2019, **48**, 12199-12209.

[17] W. Geng, H. Han, F. Liu, X. Liu, L. Xiao, W. Wu, *J. CO2 Util.,* 2017*,* **21***,* 64-71.

[18] X. Liu, Y. Song, W. Geng, H. Li, L. Xiao, W. Wu, *Catalysts*, 2016, **6**, 75.

[19] Y. Chen, S. Choi, L. T. Thompson, *J. Catal.,* 2016, **343**, 147-156.

[20] S. Posada-Pérez, P. J. Ramírez, R. A. Gutiérrez, D. J. Stacchiola, F. Viñes, P. Liu, F. Illas, J. A. Rodriguez, *Catal. Sci. Technol.,* 2016, **6**, 6766-6777.

[21] J. A. Rodriguez, P. Liu, D. J. Stacchiola, S. D. Senanayake, M. G. White, J. G. Chen, *ACS Catal*., 2015, **5, 11**, 6696–6706.

[22] M. D. Porosoff, X. Yang, J. A. Boscoboinik, J. G. Chen, *Angew. Chem*., 2014, **126**, 6823-6827.

[23] S. Posada-Pérez, F. Viñes, P. J. Ramirez, A. B. Vidal, J. A. Rodriguez, F. Illas, *Phys. Chem. Chem. Phys*., 2014, **16**, 14912-14921.

[24] X. Ma, C. Ren, H. Li, X. Liu, X. Li, K. Han, W. Li, Y. Zhan, A. Khan, Z. Chang, C. Sun, H. Zhou, *J. Colloid. Interf. Sci.,* 2021, **582**, 488-495.

[25] J. Dong, Y. Shi, C. Huang, Q. Wu, T. Zeng, W. A. Yao, *Appl. Catal. B-Environ*., 2019, **243**, 27-35.

[26] X. Yue, S. Yi, R. Wang, Z. Zhang, S. Qiu, *Nano Energy*, 2018, **47**, 463-473.

[27] Y. X. Pan, J. B. Peng, S. Xin, Y. You, Y. L. Men, F. Zhang, M. Y. Duan, Y. Cui, Z. Q. Sun, J. Song, *ACS Sustainable Chem. Eng.,* 2017, **5, 6,** 5449-5456.

[28] B. Ma, X. Wang, K. Lin, J. Li, Y. Liu, H. Zhan, W. Liu, *Int. J. Hydrogen Energ*., 2017, **42, 30**, 18977-18984.

[29] Y. Wang, W. Tu, J. Hong, W. Zhang, R. Xu, *Journal of Materiomics*, 2016, **2, 4,** 344-349.

[30] A. M. Alexander, J. S. J. Hargreaves, *Alloys. Chem. Soc. Rev*., 2010, **39,** 4388−4401.

[31] J. Liu, G. Hodes, J. Yan, S. Liu, *Chinese J. Catal.,* 2021, **42**, 205-216.

[32] X. Yue, S. Yi, R. Wang, Z. Zhang, S. A. Shilun Qiu*, J. Mater. Chem. A*., 2017, **5***,* 10591-10598.

[33] H. Li, W. Hong, Y. Cui, S. Fan, L. Zhu, *J. Alloy. Compd.,* 2013*,* **569**, 45–51.

[34] N. Wang, X. Zhang, Y. Wang, W. Yu, H. L. W. Chan, *Lab. Chip*., 2014, **14**, 1074–1082.

[35] O. Oluwafunmilola, M. M. Maroto-Valer, *J. Photoch. Photobio*. C., 2015, **24**, 16-42.

[36] L. Li, R. Chen, Q. Liao, X. Zhu, G. Wang, D. Wang, *Int. J. Hydrogen Energ.*. 2014, **39**, 19270-19276.

[37] L. Li, R. Chen, X. Zhu, H. Wang, Y.Z. Wang, Q. Liao, D.Y. Wang, *ACS Appl. Mater. Inter*., 2013, **5**, 12548-12553.

[38] J. Albo, M. I. Qadir, M. Samperi, J. A. Fernandes, I. de Pedro, J. Dupont, *Chem. Eng. J*., 2021, **404**, 126643.

[39] M. Cheng, Y. Huang, R. Gao, S. Bai1, *Catal. Lett.,* 2019, **149**, 3000–3011.

[40] M. Cheng, S. Yang, R. Chen, X. Zhu, Q. Liao, Y. Huang, *Int. J. Hydrogen Energ*., 2017, **42(15)**, 9722-9732.

[41] X. Cheng, R. Cheng, X. Zhu, Q. Liao, L. An, D. Ye, X. He, S. Li, *Energy*, 2017, **120**, 267–282.

[42] R. Chen, X. Cheng, X. Zhu, Q. Liao, L. An, D. Ye, X. He, Z. Wang, *Chem. Eng. J*., 2017, **316**, 911–918.

[43] X. Cheng, R. Chen, X. Zhu, Q. Liao, X. He, S. Li, L. Li, *Int. J. Hydrogen Energ*., 2016, **41**, 2457–2465.

[44] G. García, M. Roca-Ayats, O. Guillén-Villafuerte, J. L. Rodríguez, M. C. Arévalo, E. Pastor, *J. Electroanal. Chem*., 2017, **793**, 235–241.

[45] G. García, O. Guillén-Villafuerte, J. L. Rodríguez, M. C. Arévalo, E. Pastor, *Int. J. Hydrogen Energ*., 2016, **41 (43)**, 19664–19673.

[46] R. Guil-López, E. Nieto, J. A. Botas, J. L. G. Fierro, *J. Solid State Chem*., 2012, **190**, 285–295.

[47] J. Albo, A. Irabien, *J. Catal.,* 2016, **343**, 232–239.

[48] J. Albo, A. Saez, J. Solla-Gullon, V. Montiel, A. Irabien, *Appl. Catal. B-Environ*., 2015, **176–177**, 709-717.

[49] H. Cheng, J. Wang, Y. Zhao, X. Han, *RSC Adv*., 2014, **4**, 47031-47038.

[50] G. C. Vázquez, M. A. Peche-Herrero, D. Maestre, B. Alemán, J. Ramírez-Castellanos, A. Cremades, J. M. Gonzalez-Calbet, J. Piqueras, J*J. Mater. Chem. C*., 2014, **2***, 48*, 10377–10385.

[51] P. Russo, R. Liang, R. X. He, Y. N. Zhou, *Nanoscale*, 2017, **9, 18**, 6167–6177.

[52] W. F. Zhang, M. S. Zhang, Z. Yin, Q. Chen, *Appl. Phys. B*., 2000, **70***, 2*, 261–265.

[53] Y. L. Men, Y. You, Y. X. Pan, H. Gao, Y. Xia, D. G. Cheng, J. Song, D. X. Cui, N. Wu, Y. Li, S. Xin, J. B. Goodenough, *J. Am. Chem. Soc.,* 2018, **140**, *40,* 13071-13077.

[54] P. Li, H. Hu, J. Xu, H. Jing, H. Peng, J. Lu, C. Wu, *Appl. Catal. B-Environ*., 2014, **147**, 912-929.

[55] H. Wang, L. Zhang, K. Wang, X. Sun, W. Wang, *Appl. Catal. B-Environ*., 2019, **243**, 771-779.

[56] P. Y. Jia, R. T. Guo, W. G. Pan, C. Y. Huang, J. Y. Tang, X. Y. Liu, H. Qin, Q. Y. Xu, *Colloid Surface A*., 2019, **570**, 306-316.

[57] R. Zhang, P. Li, F. Wang, L. Ye, A. Gaur, Z. Huang, Z. Zhao, Y. Bai, Y. Zhou, *Appl. Catal. B-Environ*., 2019, **250**, 273-279.

[58] Y. Wang, Y. Xu, Y. Wang, H. Qin, X. Li, Y. Zuo, S. Kang, L. Cui, *Catal. Commun*., 2016, **74**, 75-79.

[59] N. H. Nguyen, H. Y. Wu, H. Bai, H., *Chem. Eng. J*., 2015, **269**, 60-66.

[60] H. Y. Wu, N. H. Nguyen, H. Bai, S. M. Chang, J. C. S. Wu, *RSC Adv.,* 2015, **5**, 63142-63151.

[61] S. Meister, R. O. Reithmeier, M. Tschurl, U. Heiz, B. Rieger, *ChemCatChem*, 2015, **7**, 690-697.